Static and dynamic imaging performance analysis of pentagonal pixel array detector

FAN WANG*, HUI TIAN, JINPING NI, FEI HOU, TONG YANG, RONGLI GUO
Xi'an Technological University, School of Optoelectronics Engineering, Xi'an, 710021, China

To analyze the imaging performance of pentagonal-shaped pixel array detectors, static and dynamic modulation transfer functions (MTFs) are established. To obtain the static MTF, the analytical expressions of both the aperture function and sampling function are first determined, and then, the static MTF of the detector is deduced according to its definition. In addition, the dynamic MTF of the detector for linear motion imaging is established. The results showed that static MTF values of the pentagonal pixel array detector are clearly larger than the values at the same frequencies along the *y* direction for other rectangular, hexagonal and triangular pixel array detectors, while they are almost similar along the *x* direction. In addition, the pentagonal pixel array detector has six zeroless directions, which can help enhance the image quality with image processing methods. The dynamic imaging performance with different motion parameters is also analyzed according to the established dynamic MTF. Both static and dynamic MTFs can help optimize the design of new specially shaped pixel array detectors and evaluate their imaging performance.

(Received August 27, 2019; accepted August 18, 2020)

Keywords: Specially shaped pixel, Pentagonal pixel, Array detector, Modulation transfer function

1. Introduction

Human eyes are highly adaptive imaging devices that can make tradeoffs between high resolution, low data volume and a wide field of view (FOV). In addition, the human vision system has unique features such as parallel processing and small involuntary movement. Thus, many works have been carried out to develop and design bionic imaging sensors. Due to the development of silicon-based CMOS technology, various bionic imaging sensors can be fabricated to improve imaging performance, such as retina-like sensors [1-3], which are more suitable for panoramic imaging and forward motion imaging, hemispherical electronic eye cameras [4] and highly curved image sensors [5]. In 2017, Guenter et al. successfully designed a highly curved image sensor to improve the modulation transfer function and relative illumination, especially at the edges of the image field [5]. In addition, specially shaped pixel array detectors, such as pentagonal pixel array detectors, have been designed for special purposes. When compared to a circular pixel, a pentagonal pixel can be more easily fabricated in practice due to the masking pattern used in photolithography [6], as a straight line is used instead of a curved line.

A traditional imaging detector has pixels with rectangular shapes. Usually, a modulation transfer function (MTF) is adopted to evaluate the imaging performance [7-10]. MTF models for these detectors are easily deduced and have been well studied [11-14]. The MTFs of nonrectangular pixel array detectors, such as triangular pixel array detectors and trapezoidal pixel array detectors [15-17], have also been studied. We can obtain the frequency response of nonrectangular pixel array detectors from their MTFs. For example, a trapezoidal pixel array detector has six zeroless directions in the frequency domain, while a rectangular array does not have a zeroless direction. Hence, these results can be used to analyze whether the detector is suitable for a given application.

In this paper, a method for deducing both the static and dynamic MTFs of a pentagonal pixel shape array detector is proposed. First, the aperture function and sampling function are determined according to the pixel geometry shape and the arrangement of the pixels. Then, the static MTF model of the pentagonal pixel array detector can be obtained according to its definition, and the two–dimensional MTF curves are plotted. Based on this result, the MTF is compared to that of the rectangular, triangular and hexagonal pixel array detectors with the same pixel areas. In addition, to evaluate the MTF performance in dynamic imaging, such as vision tracking, the dynamic MTF is also deduced according to the motion feature.

2. Static MTF model of pentagonal pixel array detector

The MTF is the modulus of the optical transfer function (OTF). Hence, we first need to determine the expression of the OTF. According to the definition, the expression of the OTF is the ratio between the spectra of output and input images. Thus, the output and input image spectrum need to be calculated in advance. In the following, we first obtain the expression of the output image.

For an arbitrary pixel shape array detector, according to the sampling theorem, the output image can be expressed as:

$$o(x,y)=[s_{in}(x,y)*A(x,y)]samp(x,y)rect(\frac{x}{w},\frac{y}{w}) \tag{1}$$

where $o(x, y)$ and $s_{in}(x, y)$ are the output and input images, respectively. Symbol $A(x, y)$ denotes the pixel aperture function, and $samp(x, y)$ is the sampling function. The last item in Eq. (1) is determined by the size of the sensor, with dimensions of $w \times w$. The symbol "*" represents the convolution operation. The pixel aperture function is determined by the pixel shape, while the sampling function is dependent on the pixel arrangement. In Eq. (1), the expression of the output image is clearly a function of the input image.

The output and input image spectra can be obtained by the Fourier transformation of the output and input images, respectively. Based on the definition of the OTF, this can be calculated by normalizing the ratio between the output and input image spectrum:

$$OTF(u,v)=\frac{O(u,v)/S_{in}(u,v)}{O(0,0)/S_{in}(0,0)} \tag{2}$$

where $O(u, v)$ and $S_{in}(u, v)$ are the output and input image spectra, respectively.

The MTF is the modulus of the optical transfer function, so its expression is:

$$MTF(u,v)=\left|\frac{O(u,v)/S_{in}(u,v)}{O(0,0)/S_{in}(0,0)}\right| \tag{3}$$

From Eqs. (1-3), if we want to obtain the expression of the MTF, the aperture function $A(x, y)$ and sampling function $samp(x, y)$ need to be determined in advance.

To determine the aperture function and sampling function, the pixel arrangement of the detector is depicted in Fig. 1. The pixels are arranged in such a way as to make the blind area as small as possible.

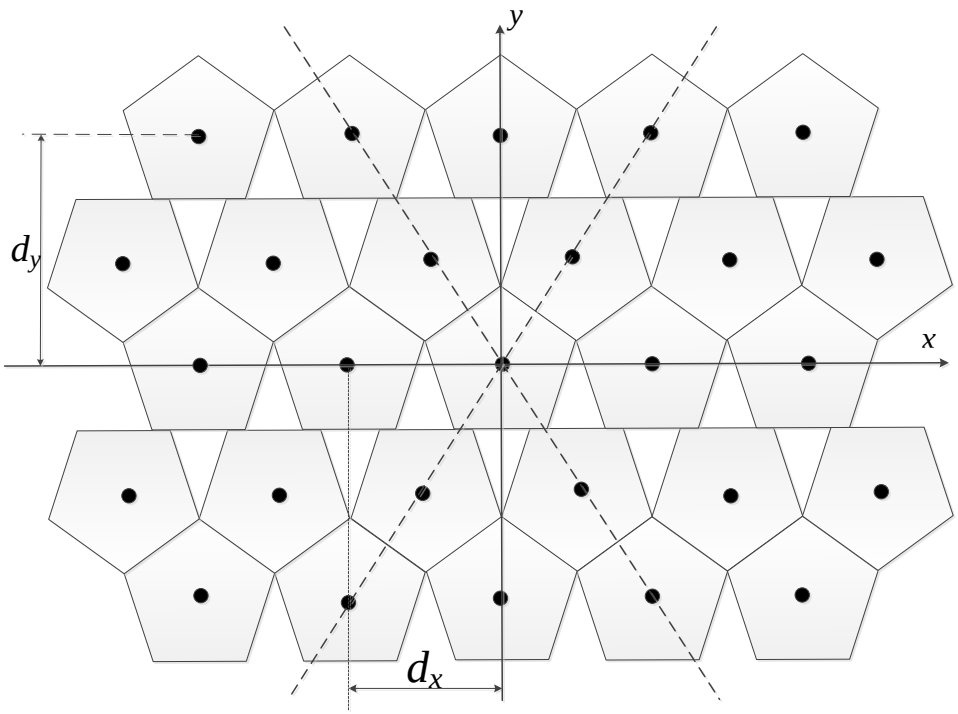

Fig. 1. Diagram of a pentagonal pixel array detector

In addition, the geometric parameters of a pentagonal pixel are shown in Fig. 2. The pixel's side length is a, and each interior angle is 108°. For simplicity, the pixel is assumed to have a 100% fill factor [15, 17]. According to Fig. 2, the aperture function of the pentagonal pixel array detector is [15]:

$$A_{pen}(x,y)=\begin{cases}\dfrac{1}{A_s} & (x,y)\in s\\ 0 & (x,y)\in s\end{cases} \tag{4}$$

Here, s represents the photosensitive region of a pixel. Symbol A_s is the area of the photosensitive region and $A_s=\dfrac{5a^2}{4\tan(36^\circ)}$ (and we assume that the response of each pixel is the same).

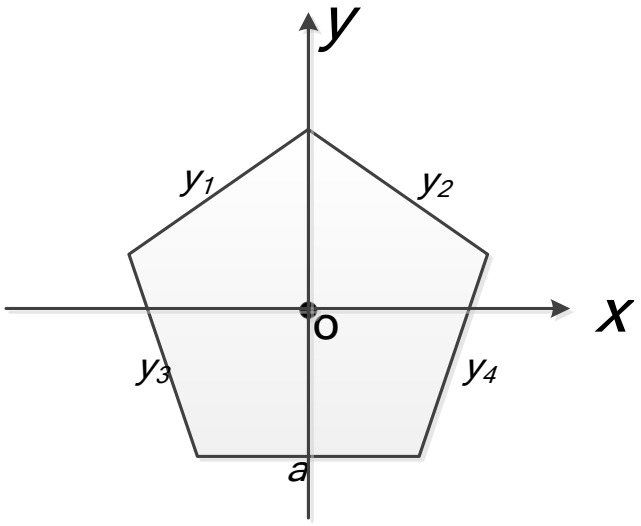

Fig. 2. Geometric parameters of a pentagonal pixel

According to the coordinates shown in Fig. 2, the equations of the four sides of the pentagonal pixel are:

$$\begin{cases}y_1=\tan(36^\circ)\cdot x+\dfrac{a}{2\sin(36^\circ)}\\ y_2=-\tan(36^\circ)\cdot x+\dfrac{a}{2\sin(36^\circ)}\\ y_3=-\dfrac{2\cos(18^\circ)}{2\cos(36^\circ)-1}x+\dfrac{a\cos(18^\circ)}{2\cos(36^\circ)-1}+\dfrac{a}{2\tan(36^\circ)}\\ y_4=\dfrac{2\cos(18^\circ)}{2\cos(36^\circ)-1}x+\dfrac{a\cos(18^\circ)}{2\cos(36^\circ)-1}+\dfrac{a}{2\tan(36^\circ)}\\ y_{triangle}\in\left[\dfrac{a}{4\cos(18^\circ)},\quad\dfrac{a}{2\sin(36^\circ)}\right]\\ y_{trapezoid}\in\left[-\dfrac{a}{2\tan(36^\circ)},\quad\dfrac{a}{4\cos(18^\circ)}\right]\end{cases} \tag{5}$$

According to the sampling position shown in Fig. 1, the sampling function of the pentagonal pixel array detector can be expressed as:

$$samp(x,y)=comb\left(\frac{x}{d_x}+\frac{y}{d_y},\frac{x}{d_x}-\frac{y}{d_y}\right) \tag{6}$$

where

$$d_x=2a\sin(36^\circ);d_y=a\cos(18^\circ)+\frac{a}{2\tan(36^\circ)}+\frac{a}{2\sin(36^\circ)}$$

According to Eq. (1), for the arbitrary input image, the output image of the detector is:

$$\begin{aligned}o_{pen}(x,y)&=[s_{in}(x,y)*t_{pen}(x,y)]\times\\ &\times comb(\frac{x}{d_x}+\frac{y}{d_y},\frac{x}{d_x}-\frac{y}{d_y})\times rect(\frac{x}{w},\frac{y}{w})\end{aligned} \tag{7}$$

where the subscript *pen* denotes pentagonal pixels. By using Fourier transformation, the spectrum of the output image is:

$$
\begin{aligned}
&o_{pen}(u,v) = FT\{O_{pen}(x,y)\} \\
&= \int_{-\infty}^{\infty}\int_{-\infty}^{\infty} [s_{in}(x,y) * t_{pen}(x,y)] \times comb\left(\frac{x}{d_x}+\frac{y}{d_y}, \frac{x}{d_x}-\frac{y}{d_y}\right) \times rect\left(\frac{x}{w}, \frac{y}{w}\right) e^{-2\pi iux} e^{-2\pi ivy} dxdy \\
&= S(u,v) \times \left\{ \int_{\frac{a}{4\cos(18^\circ)}}^{\frac{a}{2\sin(36^\circ)}} \int_{-\frac{y}{\tan(36^\circ)}+\frac{a}{2\sin(36^\circ)\tan(36^\circ)}}^{\frac{y}{\tan(36^\circ)}-\frac{a}{2\sin(36^\circ)\tan(36^\circ)}} e^{-2\pi iux} e^{-2\pi ivy} dxdy + \right. \\
&\left. + \int_{-\frac{a}{2\tan(36^\circ)}}^{\frac{a}{4\cos(18^\circ)}} \int_{\frac{y[2\cos(36^\circ)-1]}{-\cos(18^\circ)}+a+\frac{a[2\cos(36^\circ)-1]}{4\tan(36^\circ)\cos(18^\circ)}}^{\frac{y[2\cos(36^\circ)-1]}{\cos(18^\circ)}+a+\frac{a[2\cos(36^\circ)-1]}{4\tan(36^\circ)\cos(18^\circ)}} e^{-2\pi iux} e^{-2\pi ivy} dxdy \right\} \\
&\quad * comb\left(\frac{d_x}{2}u+\frac{d_y}{2}v, \frac{d_x}{2}u-\frac{d_y}{2}v\right) * \mathrm{sinc}(wu, wv)
\end{aligned}
\tag{8}
$$

Here, FT{ } denotes the Fourier transformation.

If the input image is band-limited within a certain region determined by the sampling function, it can be exactly reconstructed [17]. According to refs [7, 14, 18-20], the input image can be written as:

$$
S_{in}(u,v) = 0 \qquad if \quad u^2+v^2 = \xi_N^2 \left(\xi_N = \sqrt{\frac{1}{(2d_x)^2}+\frac{1}{(2d_y)^2}} \right)
\tag{9}
$$

Here, ξ_N is the Nyquist frequency, and it represents the upper frequency limit of the input irradiance function to avoid aliasing. With this assumption, Eq. (8) can be simplified:

$$
\begin{aligned}
&o_{pen}(u,v) \approx k \times S(u,v) \\
&\quad \times \left\{ \int_{\frac{a}{4\cos(18^\circ)}}^{\frac{a}{2\sin(36^\circ)}} \int_{-\frac{y}{\tan(36^\circ)}+\frac{a}{2\sin(36^\circ)\tan(36^\circ)}}^{\frac{y}{\tan(36^\circ)}-\frac{a}{2\sin(36^\circ)\tan(36^\circ)}} e^{-2\pi iux} e^{-2\pi ivy} dxdy + \right. \\
&\left. + \int_{-\frac{a}{2\tan(36^\circ)}}^{\frac{a}{4\cos(18^\circ)}} \int_{\frac{y[2\cos(36^\circ)-1]}{-\cos(18^\circ)}+a+\frac{a[2\cos(36^\circ)-1]}{4\tan(36^\circ)\cos(18^\circ)}}^{\frac{y[2\cos(36^\circ)-1]}{\cos(18^\circ)}+a+\frac{a[2\cos(36^\circ)-1]}{4\tan(36^\circ)\cos(18^\circ)}} e^{-2\pi iux} e^{-2\pi ivy} dxdy \right\}
\end{aligned}
\tag{10}
$$

Furthermore, the integral in Eq. (10) is:

$$\int_0^{a\sin(36^\circ)}\int_{-\left(\frac{a\sin(36^\circ)-y}{\tan(36^\circ)}\right)}^{\frac{a\sin(36^\circ)-y}{\tan(36^\circ)}} e^{-2\pi iux}dxe^{-2\pi ivy}dy+\int_{-a\cos(18^\circ)}^{0}\int_{\frac{\left[\cos(36^\circ)-\frac{1}{2}\right]y}{\cos 18^\circ}+a\cos(36^\circ)}^{-\frac{\left[\cos(36^\circ)-\frac{1}{2}\right]y}{\cos 18^\circ}-a\cos(36^\circ)} e^{-2\pi iux}dxe^{-2\pi ivy}dy$$

$$=\frac{1}{4\pi^2}\left\{\frac{\frac{2}{\tan(36^\circ)}\left[\cos\left(2\pi iv\cdot\sin(36^\circ)a\right)-\cos\left(2\pi iu\cdot\cos(36^\circ)a\right)\right]}{\left(\frac{u^2}{\tan^2(36^\circ)}-v^2\right)}+2i\frac{\left[-\frac{1}{\tan(36^\circ)}\sin\left(2\pi iv\cdot\sin(36^\circ)a\right)+\frac{v}{u}\cdot\sin(\pi av)\right]}{\left(\frac{u^2}{\tan^2(36^\circ)}-v^2\right)}\right\}e^{\cdot\frac{a}{4\cos(18^\circ)}\cdot v}$$

$$+\frac{1}{4\pi^2 u}\left(\frac{e^{-2\pi iua\cos(36^\circ)}}{\frac{\left(\cos(36^\circ)-\frac{1}{2}\right)u}{\cos(18^\circ)}+v}-\frac{e^{-\pi iau}}{\frac{\left(\cos(36^\circ)-\frac{1}{2}\right)u}{\cos(18^\circ)}+v}+\left(\frac{e^{\pi i\cdot au}}{\frac{\left(\frac{1}{2}-\cos(36^\circ)\cdot u\right)}{\cos(18^\circ)}+v}-\frac{e^{-\pi i\cdot au}}{\frac{\left(\cos(36^\circ)-\frac{1}{2}\right)\cdot u}{\cos(18^\circ)}+v}\right)\cdot e^{2\pi i\cdot a\cos(18^\circ)\cdot v}\right)e^{\cdot\frac{a}{4\cos(18^\circ)}\cdot v} \tag{11}$$

By substituting Eq. (11) into Eq. (10), the exact output image spectrum $O_{pen}(u, v)$ can be obtained, and it is clearly a function of the input image spectrum. According to Eq. (3), the MTF can be calculated by dividing the spectra of the output and input images. Finally, we can obtain the following expression:

$$MTFpen(u,v)=\left|OTFpen(u,v)\right|$$

$$=\left|\begin{array}{l}\left\{\frac{1}{2\pi^2}\frac{\frac{1}{\tan(36^\circ)}\left[\cos\left(2\pi iv\cdot\sin(36^\circ)a\right)-\cos\left(2\pi iu\cdot\cos(36^\circ)a\right)\right]}{\left(\frac{u^2}{\tan^2(36^\circ)}-v^2\right)}+i\frac{\left[-\frac{1}{\tan(36^\circ)}\sin\left(2\pi iv\cdot\sin(36^\circ)a\right)+\frac{v}{u}\cdot\sin(\pi av)\right]}{\left(\frac{u^2}{\tan^2(36^\circ)}-v^2\right)}\right\}e^{\cdot\frac{a}{4\cos(18^\circ)}\cdot v}\\ +\frac{1}{4\pi^2 u}\left(\frac{e^{-2\pi iua\cos(36^\circ)}}{\frac{\left(\cos(36^\circ)-\frac{1}{2}\right)u}{\cos(18^\circ)}+v}-\frac{e^{-\pi i\cdot au}}{\frac{\left(\cos(36^\circ)-\frac{1}{2}\right)u}{\cos(18^\circ)}+v}+\left(\frac{e^{\pi i\cdot au}}{\frac{\left(\frac{1}{2}-\cos(36^\circ)\cdot u\right)}{\cos(18^\circ)}+v}-\frac{e^{-\pi i\cdot au}}{\frac{\left(\cos(36^\circ)-\frac{1}{2}\right)\cdot u}{\cos(18^\circ)}+v}\right)\cdot e^{2\pi i\cdot a\cos(18^\circ)\cdot v}\right)e^{\cdot\frac{a}{4\cos(18^\circ)}\cdot v}\end{array}\right| \tag{12}$$

According to Eq. (12), once the length of the detector is determined, the MTF values at any frequency can be calculated.

3. Dynamic MTF model of the pentagonal pixel array detector

For the purpose of evaluating the performance of a pentagonal pixel array detector when it is used for imaging dynamic targets, such as in a situation where a target is moving linearly in the image plane, we need to establish its dynamic MTF.

According to ref. [2], the dynamic output image can be written as:

$$o_d(x,y)=[\int_0^T s_{in}[x-x_0(t),y-y_0(t)]dt * A(x,y)]samp(x,y)rect(\frac{x}{w},\frac{y}{w}) \tag{13}$$

where x_0 and y_0 are two motion parameters that are expressed as:

$$\begin{cases} x_0(t)=l_x t/T \\ y_0(t)=l_y t/T \end{cases} \tag{14}$$

where t denotes the moving time of the object and for a frame of image $t \leq T$ (symbol T is the integration time of the detector). l_x and l_y are the maximum moving distances of the image along the x and y directions, respectively, on the sensor plane during the integration time. In other words, the moving distance along the x direction is l_x and along the y direction is l_y when $t=T$. If the object is only moving along the x direction, the moving distance $l_y=0$, and *vice versa*.

The Fourier transformation of Eq. (13) is:

$$O_{dpen}(u,v) \approx k \times \int_0^T S(u,v)e^{-j2\pi[ux_0(t)+vy_0(t)]}dt \times \left\{ \int_{\frac{a}{4\cos(18^\circ)}}^{\frac{a}{2\sin(36^\circ)}} \int_{-\frac{y}{\tan(36^\circ)}+\frac{a}{2\sin(36^\circ)\tan(36^\circ)}}^{\frac{y}{\tan(36^\circ)}-\frac{a}{2\sin(36^\circ)\tan(36^\circ)}} e^{-2\pi iux_e-2\pi ivy_e}dxdy + \int_{-\frac{a}{2\tan(36^\circ)}}^{\frac{a}{4\cos(18^\circ)}} \int_{\frac{y[2\cos(36^\circ)-1]}{-\cos(18^\circ)}+a+\frac{a[2\cos(36^\circ)-1]}{4\tan(36^\circ)\cos(18^\circ)}}^{\frac{y[2\cos(36^\circ)-1]}{\cos(18^\circ)}+a+\frac{a[2\cos(36^\circ)-1]}{4\tan(36^\circ)\cos(18^\circ)}} e^{-2\pi iux_e-2\pi ivy_e}dxdy \right\} \tag{15}$$

Based on the definition of the DMTF:

$$DMTF_{pen}(u,v)=MTF_{pen}(u,v)\times T \times \sin c[\pi(ul_x+vl_y)]\exp[-j\pi(ul_x+vl_y)] \tag{16}$$

If the motion parameters T, lx and ly are determined, the DMTF can be analyzed quantitatively.

4. Analysis and comparison

Given that the geometric parameters of the detector are provided, both the static and dynamic MTFs of the pentagonal pixel array detector can be established. Then, the MTF and DMTF curves can be plotted. We can analyze the imaging features of the pentagonal pixel array detector and then compare its features with those of other detectors.

4.1. Static MTF comparison

As long as the parameters of the pentagonal pixel array detector are determined, the exact expression of the MTF can be obtained. In the following, we first assume that the side length a of a pentagonal pixel is 10 μm, and the two-dimensional graphical representation static MTF is shown in Fig. 3 to directly demonstrate the features of its static MTF. From Fig. 3, we can clearly observe the two-dimensional MTF. The contour plot of the pentagonal pixel MTF is shown in Fig. 4.

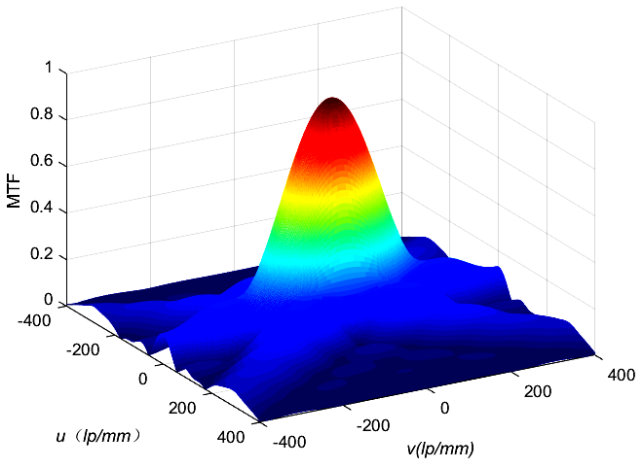

Fig. 3. MTF of a pentagonal pixel array detector

(*a=10 μm*) *(color online)*

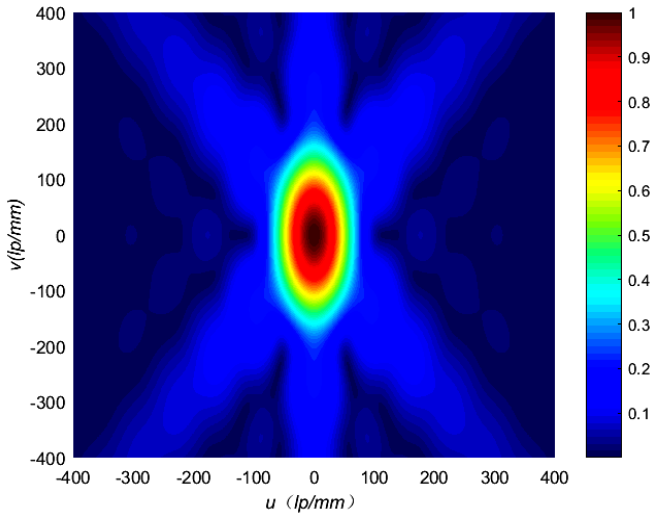

Fig. 4. Contour plot of the pentagonal pixel MTF (color online)

While analyzing the MTF of the detector with equilateral pentagonal pixels, it is observed that the MTF of the equilateral pentagonal pixels is nonzero in six directions, and it decreased gradually in these directions (Figs. 3 and 4).

These six directions are determined along three lines:

$$d_1: u=0;\ d_2: v=u/\tan(36°);\ d_3: v=-u/\tan(36°)$$

For the detector with pentagonal triangular pixels, the spatial frequency in the different directions could be helpful to the optical system resolution. In such cases, the cutoff frequency could be large. This is an interesting factor because the same situation does not occur with the rectangular detector, and the MTF of the traditional rectangular detector goes to zero in any direction.

The MTF curves along the *x* and *y* directions are given in Fig. 4 and Fig. 5, respectively. The cutoff frequency along the *x* direction is shown in Fig. 5. In Fig. 6, we cannot find the cutoff frequency, which means that the MTF values along the *y* direction are no longer zero. It is thus proven that the *y* direction is a zeroless direction.

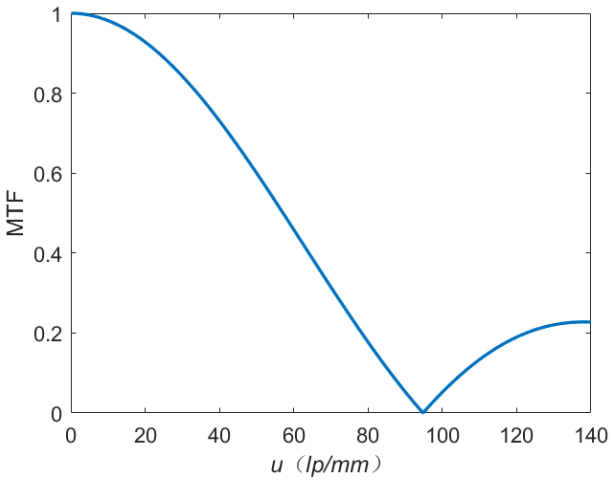

Fig. 5. 1D plot of MTF along the x direction of the pentagonal pixel array detector (a=10 μm)

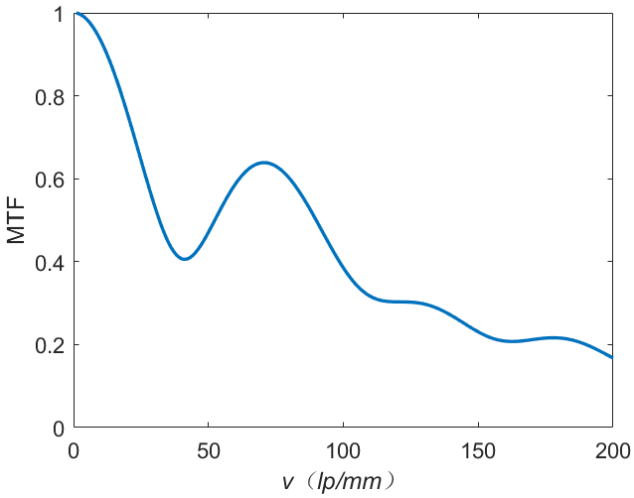

Fig. 6. 1D plot of MTF along the y direction of the pentagonal pixel array detector (a=10 μm)

Table 1. Comparison of MTF values among different pixel lengths of pentagonal pixel array detector

	u			*v*		
	10 *lp/mm*	15 *lp/mm*	20 *lp/mm*	10 *lp/mm*	15 *lp/mm*	20 *lp/mm*
10 μm	MTF=0.96	MTF=0.93	MTF=0.87	MTF=0.94	MTF=0.86	MTF=0.76
20 μm	MTF=0.87	MTF=0.73	MTF=0.56	MTF=0.78	MTF=0.54	MTF=0.41
30 μm	MTF=0.74	MTF=0.47	MTF=0.19	MTF=0.57	MTF=0.41	MTF=0.39

To compare the MTF of pentagonal pixels with different pixel sizes, the MTFs of the pentagonal pixel array detector with pixel lengths of 20 μm and 30 μm are calculated, and the results are shown in Table 1. The

table shows that MTF values decrease significantly with increasing pixel length, which is the same trend as that of the traditional pixel shape detector.

To compare the MTFs of four different pixel shapes (rectangular, triangular, hexagonal and pentagonal pixels) but with the same pixel area, the pixel arrangements and MTFs of the rectangular, triangular, and hexagonal pixel detectors are introduced in the following. The pixel arrangements are shown in Fig. 7. By using the MTF expressions of different pixel shape detectors, the MTF values at the same frequencies are calculated and compared.

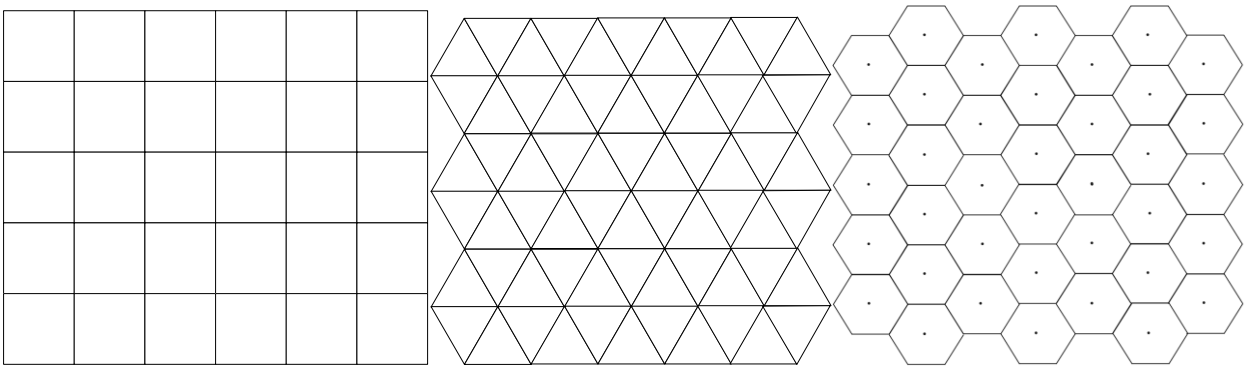

(a) rectangular pixel detector (b) triangular pixel detector (c) hexagonal pixel detector

Fig. 7. Diagram of different pixel shape detectors

4.1.1. MTF of a rectangular pixel detector

The rectangular pixel array detector is the type of detector most commonly used in imaging systems, and the square pixel array detector represents a special case. If the pixel shape is square and the length of each side of a square pixel is 2*a*, the detector MTF is:

$$MTF_{rect} = \left|\mathrm{sinc}(2au, 2av)\right| \tag{17}$$

4.1.2. MTF of a Triangular Pixel Detector

If the length of each side of a triangular pixel is *a*, then the MTF of the triangular pixel detector is:

$$MTF_{tri} = \frac{2\sqrt{[\cos(\pi av\sqrt{3}) - \cos(\pi au)]^2 + [\frac{v}{u}\sqrt{3}\sin(\pi au) - \sin(\pi av\sqrt{3})]^2}}{3\pi^2 a^2 (v^2 - \frac{u^2}{3})} \tag{18}$$

4.1.3. MTF of a hexagonal pixel detector

The MTF of a hexagonal pixel detector (its length of each side is also *a*) is:

$$MTF_{hex} = \frac{\frac{v}{u}\sin(\pi au)\sin(\pi\sqrt{3}av) - \frac{1}{\sqrt{3}}\cos(\pi au)\cos(\pi\sqrt{3}av) + \frac{1}{\sqrt{3}}\cos(2\pi au)}{\pi^2[v^2 - \left(\frac{u}{\sqrt{3}}\right)^2]} \tag{19}$$

Here, we assume that the pixel area is 100 μm^2, and then the corresponding pixel lengths can be deduced and are shown in Table 2.

Table 2. The pixel length of differently shaped pixels when the pixel area is 100 μm^2

Pixel shape	**pixel length (μm)**
Pentagonal pixel	7.62
Rectangular pixel	10
Triangular pixel	15.2
Hexagonal pixel	6.24

The cutoff frequency is the main feature of the MTF. Thus, we computed the cutoff frequencies of different pixel shapes and plotted these MTF curves along the *x* direction and *y* direction, which are shown in Fig. 8 and Fig. 9, respectively. The calculated cutoff frequencies are also shown in Table 3. It is worth noting that Figs. 8 and 9 show that the cutoff frequencies of the MTF of differently shaped pixels along the *x* direction are close to each other. As a counterpart, the MTF values of the pentagonal pixel array detector along the *y* direction are larger than those of other detectors. Moreover, the pentagonal pixel array detector has six zeroless directions. When the MTF is not explicitly zero at one point, the image quality can be enhanced with image processing methods.

Table 3. The cutoff frequencies along the x direction of different pixel shape arrays

Pixel shape	**Cutoff frequency along *x* direction (*lp/mm*)**
Pentagonal pixel	95
Rectangular pixel	100
Triangular pixel	132
Hexagonal pixel	108

4.2. Dynamic MTF

Based on the DMTF model of the pentagonal pixel array detector, the DMTF curve can be plotted once the motion parameters are given. Figs. 10 (a) and (b) demonstrate two DMTFs with two sets of parameters: l_x=l_y=0.1 mm, T=1 *s*, and l_x=l_y=0.5 mm, T=1 *s*, respectively. From Fig. 3 and Fig. 8, we know that it is clear that the DMTF values are smaller than the static MTF values at the same frequencies. The DMTF values are close to zero at higher frequencies. By comparing Fig. 10(a) and Fig. 10(b), it is also shown that the DMTF value degrades when the moving distance (l_x, l_y) becomes longer. We also calculate the two sets of DMTF values at specific frequencies, and the results are shown in Table 4. We can see from Table 4 that the DMTF values are smaller when the moving distance is longer, which means that the imaging performance will be better when the moving distance is shorter.

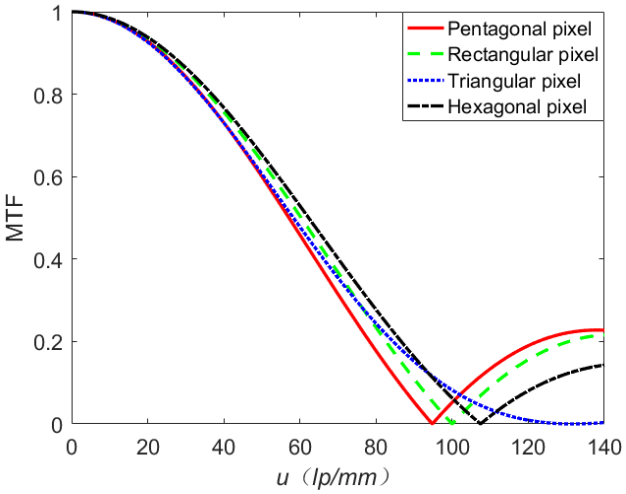

Fig. 8. MTF along the x direction of different pixel array detectors when the pixel area is 100 μm² (color online)

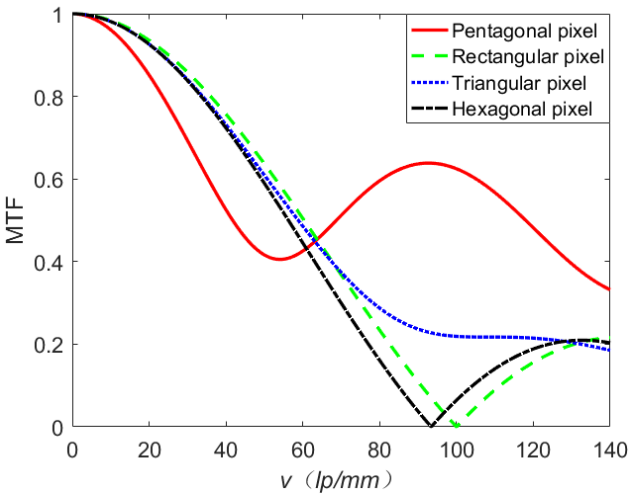

Fig. 9. MTF along the y direction of different pixel array detectors when the pixel area is 100 μm² (color online)

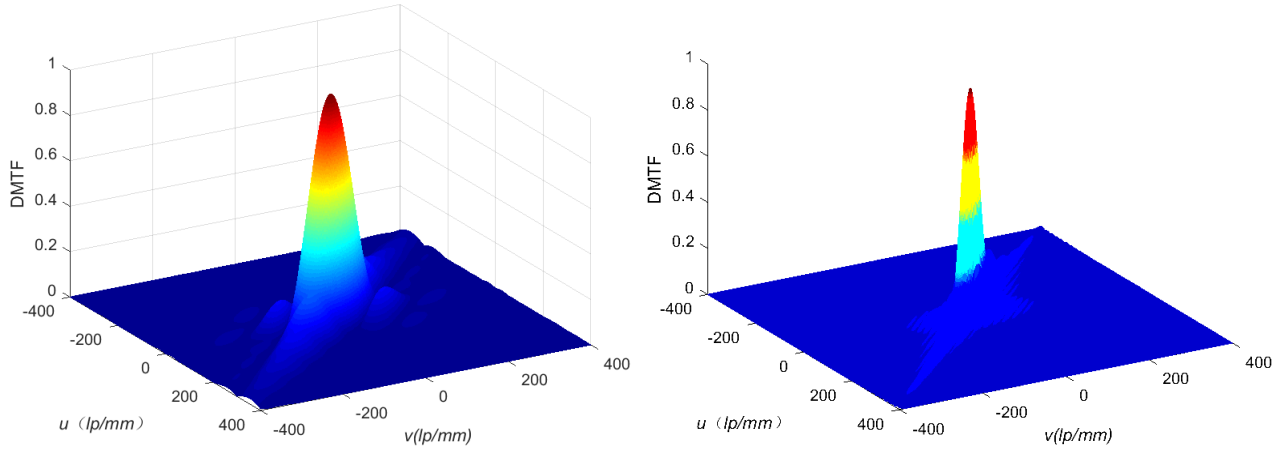

(a) (b)

Fig. 10. DMTF of a pentagonal pixel array detector (a=10 μm) (a) l_x=l_y=0.1 mm (b) l_x=l_y=0.5 mm (color online)

Table 4. Comparison of DMTF values between different motion lengths at the same frequencies

	u=2 *lp/mm* *v*=2 *lp/mm*	*u*=6 *lp/mm* *v*=6 *lp/mm*	*u*=16 *lp/mm* *v*=0 *lp/mm*	*u*=0 *lp/mm* *v*=16 *lp/mm*
l_x=l_y=0.1 mm	DMTF=0.99	DMTF=0.97	DMTF=0.94	DMTF=0.90
l_x=l_y=0.5 mm	DMTF=0.93	DMTF=0.50	DMTF=0.18	DMTF=0.17

5. Conclusion

To analyze the static and dynamic imaging ability of a pentagonal pixel array detector, we established static and dynamic MTFs. The static MTF was established according to its definition. In addition, the DMTF model for dynamic imaging was also established. Both MTF and DMTF curves were plotted. From the 2D MTF and DMTF, the imaging performances were analyzed visually and quantitatively. The results showed that the cutoff frequency of the pentagonal pixel array detector along the *x* direction was close to those of other detectors, while it exhibited better imaging performance in six zeroless directions, as these directions are nonzero in the frequency domain. The analysis of DMTF showed that it degraded notably with the increase of the moving distance of the image on the image plane.

Acknowledgments

This work was supported by the National Natural Science Foundation of China (NSFC) (Grant No. 11704302) and the Scientific Special Research Project of the Educational Department of Shaanxi Province, China (Grant No. 19JK0415).

References

[1] F. Berton, G. Sandini, G. Metta, Encyclopedia of Sensors **10**, 1 (2006).
[2] F. Wang, F. Cao, T. Bai, Q. Hao, Appl. Opt. **53** (9), 1947 (2014).
[3] J. Cao, Q. Hao, Y. Cheng, F. Zhang, Y. Peng, H. Yu, Appl. Opt. **55**(21), 5738 (2016).
[4] H. C. Ko et al., Nature **454** (7205), 748 (2008).
[5] B. Guenter et al., Opt. Express. **25**(12), 13010 (2017).
[6] J. Levinson Harry, "Principles of Lithography", SPIE Press, Washington, 2012.
[7] T. Battula et al, J. Electron. Imaging **27**(1), 013015 (2018).
[8] H. Li, S. Chen, IEEE Sens. J. **17**, 6571 (2017).
[9] Q. Tan, X. Wu, M. Zhang, L. Meng, H. Zhong, Y. Cai, L. Wang, Opt. Express. **27**, 9079 (2019).
[10] K. Ayatollah, Appl. Opt. **55**, 3045 (2016).
[11] R. H. Vollmerhausen, D. Reago, R. G. Driggers, "Analysis and Evaluation of Sampled Imaging Systems", SPIE Press, Washington, 2010.
[12] L. DeLuca, G. Cardone, Appl. Opt. **30**, 1659 (1991).
[13] T. Z. Bai, W. Q. Jin, "Principles and Techniques of Optical Imaging", Beijing Institute of Technology Press, Beijing, China, 2006.
[14] J. C. Feltz, M. A. Karim, Appl. Opt. **29**, 717 (1990).
[15] A. Karimzadeh, J. Opt. Soc. Am. A **31**, 1688 (2014).
[16] F. Wang et al., Opt. Eng. **55**(1), 013106-1 (2016).
[17] K. J. Barnard, G. D. Boreman, Opt. Eng. **30**, 1915 (1991).
[18] O. Yadid-Pecht, Opt. Eng. **39**, 859 (2000).
[19] K. M. Iftekharuddin, M. A. Karim, Opt. Eng. **32**, 2649 (1993).
[20] K. M. Hock, Opt. Eng. **34**, 1281 (1995).

*Corresponding author: wangfan@xatu.edu.cn